OPEN ACCESS

Molecular & Cell ARTICE

PAHSA protects hematopoietic stem cells from caspase-4/11-mediated pyroptosis and exhaustion

Yan Qian,[1,2,3,4,*] Qiannv Liu,[2,3,4] Yan Zhang,[2,3,4] Shuo Wang,[5] and Pengyan Xia[2,3,4,*]

*Correspondence: qiany@blsa.com.cn (Y.Q.); xiap@pku.edu.cn (P.X.)

Received: December 18, 2025; Accepted: March 24, 2026; Published Online: March 30, 2026; https://doi.org/10.59717/j.xinn-life.2026.100178

GRAPHICAL ABSTRACT

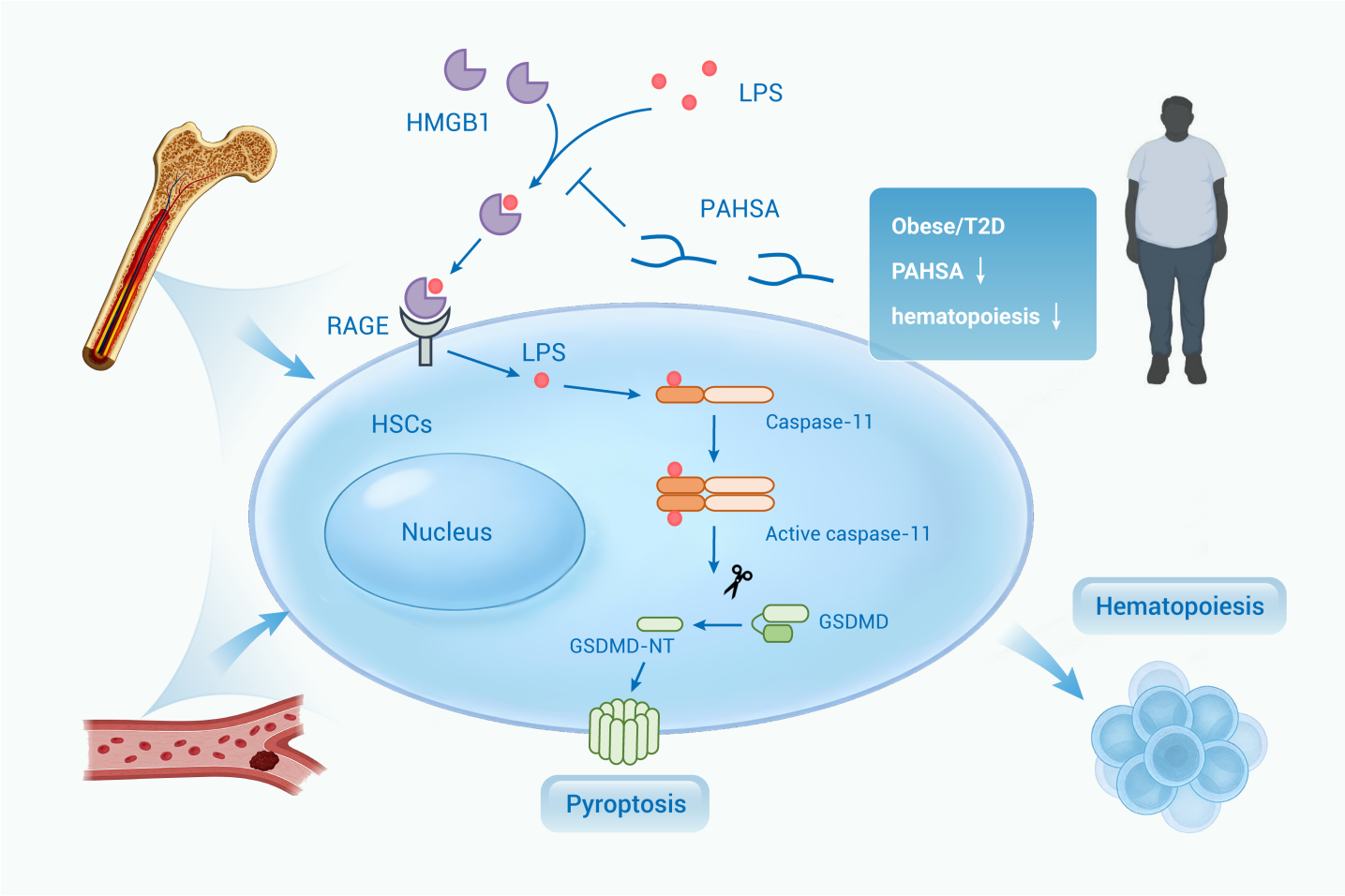

PUBLIC SUMMARY

- PAHSA protects hematopoietic stem cells (HSCs) from pyroptosis and maintains hematopoietic homeostasis.
- PAHSA inhibits LPS delivery into cytosol, blocking non-canonical inflammasome activation.
- PAHSA is potential for anti-infection treatment in obese and diabetic patients.

ARTICE Molecular & Cell

OPEN ACCESS

PAHSA protects hematopoietic stem cells from caspase-4/11-mediated pyroptosis and exhaustion

Yan Qian,[1,2,3,4,*] Qiannv Liu,[2,3,4] Yan Zhang,[2,3,4] Shuo Wang,[5] and Pengyan Xia[2,3,4,*]

[1]Beijing Life Science Academy, Beijing 102200, China

[2]Department of Immunology, School of Basic Medical Sciences, Peking University, Beijing 100191, China

[3]NHC Key Laboratory of Medical Immunology, Peking University, Beijing 100191, China

[4]Key Laboratory of Molecular Immunology, Chinese Academy of Medical Sciences, Beijing 100191, China

[5]CAS Key Laboratory of Pathogenic Microbiology and Immunology, Institute of Microbiology, Chinese Academy of Sciences, Beijing 100101, China

*Correspondence: qiany@blsa.com.cn (Y.Q.); xiap@pku.edu.cn (P.X.)

Received: December 18, 2025; Accepted: March 24, 2026; Published Online: March 30, 2026; https://doi.org/10.59717/j.xinn-life.2026.100178

Citation: Qian Y., Liu Q., Zhang Y., et al. (2026). PAHSA protects hematopoietic stem cells from caspase-4/11-mediated pyroptosis and exhaustion. *The Innovation Life* **4**:100178.

Hematopoietic stem cells (HSCs) serve as key resources of the blood system and their maintenance in the bone marrow niche is vital for the host survival. Pyroptosis following inflammasome activation is a common event when myeloid cells encounter danger signals. Whether inflammasome activation takes place in HSCs during their maintenance in the bone marrow is still elusive. Here we show that insufficient PAHSA caused by ATGL deficiency leads to increased pyroptosis and exhaustion of HSCs in *Pnpla2* knockout mice. PAHSA affects HSC viability in a cell-extrinsic manner. With the help of HMGB1, seral LPS enters HSC cytosol and induces the non-canonical inflammasome activation mediated by the caspase-4/11, leading to HSC pyroptosis and exhaustion. Seral PAHSA binds LPS and hinders LPS binding to HMGB1, thus limiting the intracellular LPS levels in HSCs. PAHSA protects HSCs from LPS-stimulated non-canonical inflammasome activation and pyroptosis in obese mice, providing a promising approach to ameliorate HSC status in obese people in the future.

INTRODUCTION

Hematopoietic stem cells (HSCs) lie in the most upstream of the hematopoietic system.[1,2] HSCs replenish the blood system through consistent self-renewal and differentiation into multipotent progenitor cells and finally mature blood cell members.[3,4] The self-renewal of HSCs is finely regulated to keep these cells capable of making numerous cells when necessary.[5-7] Chronic interleukin-1 signaling compromises the self-renewal of HSCs.[8] Prolonged LPS exposure elevates proliferative stress in HSCs.[9] HSCs expand post the uptake of free fatty acid during acute infection.[10] Moreover, pyroptosis in HSCs dominates the cytopenias caused by infection.[11,12]

Inflammasomes are immune processes that in most cases the assembly of NOD-like receptors activates caspase-1, an executor caspase that activates GSDMD to induce a form of cell death called pyroptosis.[13,14] Non-canonical inflammasomes are comprised of murine caspase-11 and human caspase-4, caspase-5, which can directly recognize LPS in the cytoplasm and cleave GSDMD further inducing pyroptosis.[15,16] Extracellular LPS binds HMGB1 and enters myeloid cell cytosol, and activates the caspase-4/11 to evoke the non-canonical inflammasome activation and pyroptosis.[17,18] HSCs are myeloid-like cells to some extent and express components involved in the non-canonical inflammasome pathway.[19,20] Whether the seral LPS enters HSC cytosol and induces the non-canonical inflammasome activation in these cells are not clear at present.

ATGL is the enzyme that catalyzes the metabolism of triacylglycerol.[21,22] Recently, ATGL is found to be a candidate enzyme for the production of branched fatty acid esters of hydroxy fatty acids (FAHFAs).[23] Palmitic-acid-9-hydroxy-stearic acid (9-PAHSA) is the most abundant branched fatty acid in mammals.[24] Branched fatty acids have anti-diabetic and anti-inflammatory effects.[24] The amount of PAHSAs is decreased in diabetic people,[25,26] leaving the question that whether these branched fatty acids have a role in the progress of diabetic progression.

Here we show that ATGL deficiency leads to diminished HSC cell numbers in mice. PAHSA binds LPS and suppresses the activation of non-canonical inflammasome in HSCs. PAHSA inhibits pyroptosis of HSCs and maintains the HSC homeostasis in obese mice. Our results uncover a protective role of PAHSA in HSC maintenance and might be useful for ameliorating the hematopoiesis in obese people in the future.

MATERIALS AND METHODS

Mice and treatments

Nlrp3$^{-/-}$ (S-KO-05210), *Casp11*$^{-/-}$ (S-KO-01332), *Gsdmd*$^{-/-}$ (S-KO-12963), *Ager*$^{flox/flox}$ (S-CKO-01095) and Vav-iCre (C001019) mice were purchased from Cyagen Biosciences (Jiangsu, China). *Pnpla2*$^{-/-}$ (NM-KO-210286) mice were from Shanghai Model Organisms (Shanghai, China). tdTomato-transgenic (007909) mice were from the Jackson Laboratory. *Ager*$^{flox/flox}$ mice were crossed with Vav-iCre mice to generate mice with *Ager* specifically deleted in HSCs. In this study, *Ager*$^{flox/flox}$;Vav-iCre mice were termed as *Ager*$^{-/-}$ mice and *Ager*$^{flox/flox}$ mice were called *Ager*$^{+/+}$ mice. tdTomato-transgenic mice were crossed with *Ager*$^{-/-}$ mice to get *Ager*$^{-/-}$ HSCs constitutively expressing the red fluorescence protein. For obese mice generation, mice were fed with a high-fat diet for 10 weeks. For antibiotics treatment, mice were administrated with drinking water containing 1 mg/ml ampicillin, 1 mg/ml gentamicin, 1 mg/ml metronidazole, 1 mg/ml neomycin, 0.5 mg/ml vancomycin, 5 g/L sucrose for one month. Mouse experiments complied with ethical regulations and were approved by the Institutional Animal Care and Use Committees at the Institute of Microbiology, Chinese Academy of Sciences.

Bone marrow transplantation

For bone marrow transplantation, sorted LT-HSCs or bone marrow nucleated cells together with 3 x 10^5 recipient bone marrow cells were intravenously injected into lethally irradiated (10 Gy) recipient mice through tail vein, followed by reconstitution examination at the proper times. Mouse experiments complied with ethical regulations and were approved by the Institutional Animal Care and Use Committees at the Institute of Microbiology, Chinese Academy of Sciences.

Cells and culture

For HSC cell culture, cells were cultured in StemPro-34 media (Invitrogen) containing 4 mM L-glutamine, 100 μg/ml streptomycin, 100 U/ml penicillin as well as the following cytokines: 10 ng/ml IL-3, 25 ng/ml SCF, 25 ng/ml Ftl-3L, 10 ng/ml GM-CSF, 25 ng/ml IL-11, 4 U/ml Epo, and 25 ng/ml Tpo. To generate BMDM cells, bone marrow cells were flushed from mouse femurs and tibias, followed by red blood cell removal using red blood cell lysis buffer. Cells were resuspended in alpha-MEM containing 10% (v/v) fetal bovine serum and 10 ng/ml M-CSF and grown at 37 °C with a 5% CO_2 humidified atmosphere for 7 days.

CFU assay

Bone marrow nucleated cells or sorted HSCs were seeded in dishes containing IMDM, supplemented with 1.2% methylcellulose (STE MCELL Technologies), 40 μM 2-mercaptoethanol, 0.5 mM haemin, 30% FBS, 2 mM l-glutamine, 20 ng/ml rmIL-3, 6 U/ml recombinant human EPO, and 20 ng/ml recombinant mouse SCF. Colonies of CFU-GM (granulocyte/macrophage), CFU-G (granulocyte), and CFU-M (macrophage) were calculated 10 days after incubation at 37 °C.

LT-CIC assay

A Long-Term Culture-Initiating Cell (LT-CIC) assay was performed using

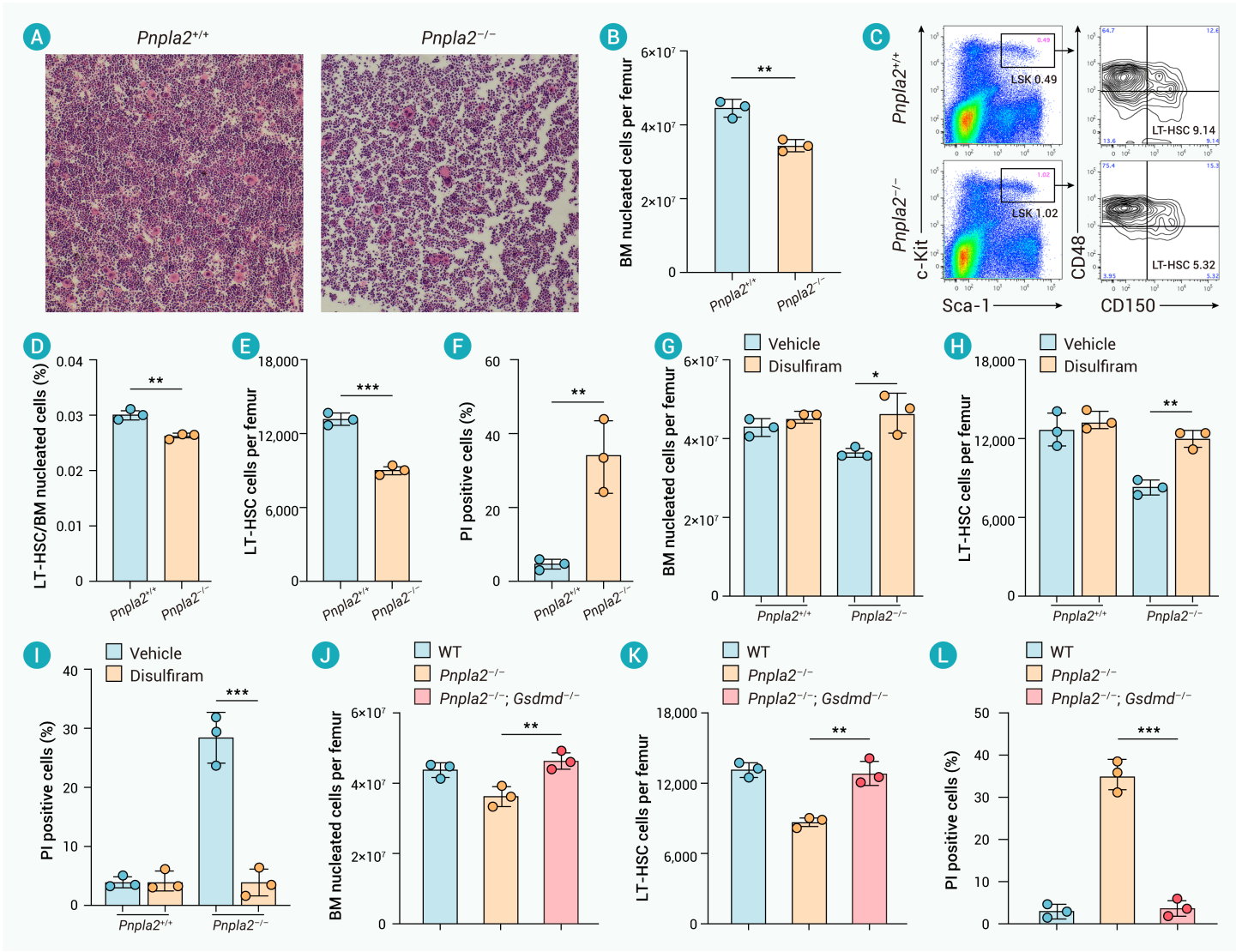

Figure 1. *Pnpla2* knockout mice have a decreased number of HSCs (A-B) Hematoxylin and eosin (H&E) staining of BM sections from *Pnpla2*$^{+/+}$ and *Pnpla2*$^{-/-}$ mice (A). Scale bar, 100 μm. Cell numbers of bone marrow nucleated cells (BMNC) were calculated using a flow cytometer (B). (C) Flow cytometric analysis of BM HSCs in *Pnpla2*$^{+/+}$ and *Pnpla2*$^{-/-}$ mice at 8 weeks of age. Sca-1^{+}c-Kit^{+} cells in the Lin^{-} and IL-7Rα^{-} population were gated out for the LT-HSC analysis. (D) The percentages of LT-HSCs in the bone marrow nucleated cells were calculated. (E) The cell numbers of LT-HSCs in one femur of the indicated mice were shown. (F) Sorted LT-HSCs were stained with propidium iodide (PI) and the percentages of PI positive cells were calculated. (G–I) *Pnpla2*$^{+/+}$ and *Pnpla2*$^{-/-}$ mice were administrated with 150 mg/ml disulfiram through drinking water for one month. The cell numbers of BMNCs were calculated using a flow cytometer (G). The cell numbers of LT-HSCs in one femur of the indicated mice were calculated using a flow cytometer (H). LT-HSCs sorted from the indicated mice were stained with PI and the percentages of PI positive cells were calculated (I). (J–L) *Pnpla2*$^{-/-}$ mice were crossed with *Gsdmd*$^{-/-}$ mice to get the mice deficient for both *Pnpla2* and *Gsdmd*. The cell numbers of BMNCs were calculated using a flow cytometer (J). The cell numbers of LT-HSCs in one femur of the indicated mice were calculated using a flow cytometer (K). LT-HSCs sorted from the indicated mice were stained with PI and the percentages of PI positive cells were calculated (L). Data were shown as means ± SD. *, $P < 0.05$; **, $P < 0.01$; ***, $P < 0.001$. Experiments were repeated three times with similar results.

primary bone marrow cells as feeder layer cells. For feeder layer cell generation, bone marrow nucleated cells were mixed with hydrocortisone-containing MyeloCult M5300 media (LTCM) and plated on to culture dishes at a concentration of 1 x 10^6 cells/cm^2. Culture media were half replaced with fresh LTCM once a week for 2–3 weeks until the culture adhesive layer has been established with an about 80% fusion. Feeder cells were then radiated at a dose of 1500 cGy. For long-term culture of initiating cells, bone marrow cells or sorted HSCs were supplemented in LTCM and plated on dishes with established feeder layer cells. 2 weeks later, cells were digested. Cells with a lymphoid morphology were collected through a flow cytometric cell sorter and subjected to a CFU assay.

Non-canonical inflammasome induction

For non-canonical inflammasome activation, *in vitro* cultured cells were incubated with 1 mg/ml LPS and 1 mg/ml HMGB1 protein, followed by PI staining and ASC specks examination. Cells were grown at 37 °C with a 5% CO_2 humidified atmosphere.

RESULTS

Pnpla2 knockout induces pyroptosis in HSCs

ATGL is responsible for the branched fatty acid production in mammalian cells.[23] Its role in the hematopoiesis has not been explored. We therefore examined the effect of *Pnpla2* (the gene encoding ATGL) deficiency on the hematopoietic system (Figure S1A). We found that the bone marrow cellularity of *Pnpla2* deficient mice were severely reduced when compared with that of wild-type controls (Figures 1A & B). In the bone marrow, the percentage of long-term HSC (LT-HSC) cells in the lineage^{-}Sca-1^{+}c-Kit^{+} (LSK) subgroup was decreased in *Pnpla2* knockout mice (Figure 1C). Consistently, the percentage of LT-HSCs in the bone marrow and the total number of LT-HSCs were also diminished in *Pnpla2* deficient mice (Figures 1D & E). When we looked at the status of cell viabilities in LT-HSCs, we found that the percentage of propidium iodide (PI) positive cells was higher in *Pnpla2* deficient cells than that in wild-type ones (Figure 1F). Pyroptosis is involved in HSC regulation during infections.[27] We then stained these HSCs with an antibody against ASC, an essential regulator of inflammasomes, whose aggregation is a hallmark of the inflammasome activation. We found that there were more cells

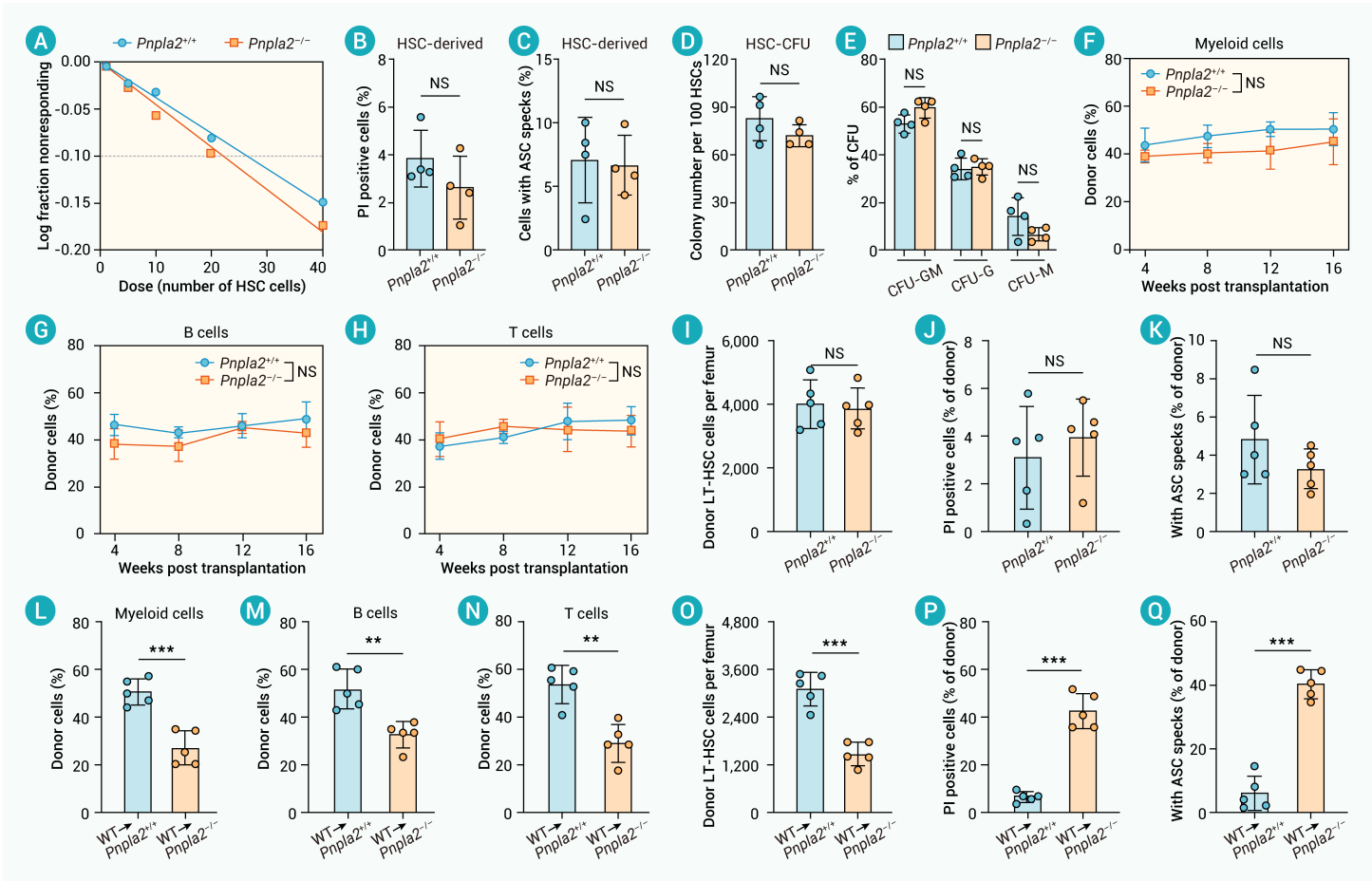

Figure 2. ATGL affects HSC self-renewal in a cell-extrinsic manner (A) A long-term culture initiating cell (LT-CIC) assay of *Pnpla2*$^{+/+}$ and *Pnpla2*$^{-/-}$ LT-HSCs. Sorted HSCs were plated onto irradiated feeder cells for 4 weeks, followed by colony forming units (CFU) determination. (B-C) LT-HSCs were plated onto irradiated feeder cells for 4 weeks, followed by digestion into a single cell suspension. Cells with a lymphoid morphology were sorted through a flow cytometric cell sorter. Cells were stained with PI and the percentages of PI positive cells were calculated (B). Cells were also stained with antibody against ASC and the percentages of cells with ASC specks were calculated (C). (D-E) LT-HSCs sorted from *Pnpla2*$^{+/+}$ and *Pnpla2*$^{-/-}$ mice were cultured *in vitro* for CFU determination. CFUs were calculated (D) and the compositions of CFU colonies were examined (E). CFU-GM for granulocyte/macrophage, CFU-G for granulocyte and CFU-M for macrophage. (F–H) 100 LT-HSCs sorted from *Pnpla2*$^{+/+}$ and *Pnpla2*$^{-/-}$ mice were co-transplanted with 3 x 10^5 CD45.1 BMNCs into lethally irradiated WT CD45.1 mice, followed by donor chimerism examination at the indicated time points. Surface markers were: Gr-1 for myeloid cells, B220 for B cells, and CD3 for T cells. (I–K) 100 LT-HSCs sorted from *Pnpla2*$^{+/+}$ and *Pnpla2*$^{-/-}$ mice were co-transplanted with 3 x 10^5 CD45.1 BMNCs into lethally irradiated WT CD45.1 mice for 16 weeks. Cell numbers of donor-derived LT-HSC in one femur of the recipient mice were calculated (I). Donor-derived LT-HSCs were stained with PI and the percentages of PI positive cells were calculated (J). Donor-derived LT-HSCs were also stained with antibody against ASC and the percentages of cells with ASC specks were calculated (K). (L–N) 100 LT-HSCs sorted from WT CD45.1 mice were co-transplanted with 3 x 10^5 *Pnpla2*$^{+/+}$ or *Pnpla2*$^{-/-}$ BMNCs into lethally irradiated *Pnpla2*$^{+/+}$ or *Pnpla2*$^{-/-}$ mice, followed by donor chimerism examination 4 weeks later. (O–Q) 100 LT-HSCs sorted from WT CD45.1 mice were co-transplanted with 3 x 10^5 *Pnpla2*$^{+/+}$ or *Pnpla2*$^{-/-}$ BMNCs into lethally irradiated *Pnpla2*$^{+/+}$ or *Pnpla2*$^{-/-}$ mice for 4 weeks. Cell numbers of donor-derived LT-HSCs in one femur of the recipient mice were calculated (O). Donor-derived LT-HSCs were stained with PI and the percentages of PI positive cells were calculated (P). Donor-derived LT-HSCs were also stained with antibody against ASC and the percentages of cells with ASC specks were calculated (Q). NS, non-significant. Data were shown as means ± SD. **, $P < 0.01$; ***, $P < 0.001$. Experiments were repeated three times with similar results.

with ASC specks in *Pnpla2* deficient cells than control ones (Figure S1B), suggesting that inflammasomes were activated in *Pnpla2* knockout HSCs.

GSDMD triggers pore formation on cell membranes to induce pyroptosis during inflammasome activation.[28,29] To find out the role of GSDMD in *Pnpla2* knockout HSCs, we treated *Pnpla2* deficient mice with disulfiram, an FDA-approved drug that blocks GSDMD pore formation on membranes.[30,31] Disulfiram treatment restored the bone marrow cellularity and LT-HSC cell number in *Pnpla2*$^{-/-}$ mice (Figures 1G & H). Disulfiram also protected HSCs from pyroptosis in *Pnpla2*$^{-/-}$ mice (Figures 1I & S1C). We then generated mice deficient for both *Pnpla2* and *Gsdmd* (Figure S1D). We found that *Gsdmd* deficiency restored the cell number of *Pnpla2*$^{-/-}$ bone marrows to a level similar to that of wild-type ones (Figure 1J). LT-HSC cell number in *Pnpla2* and *Gsdmd* double knockout mice was also elevated to a degree comparable to that of wild-type controls (Figure 1K). Consistently, cells undergoing pyroptosis were diminished in these double knockout HSCs when compared with *Pnpla2*$^{-/-}$ cells (Figures 1L & S1E). However, NLRP3 was not involved in the inflammasome activation of *Pnpla2*$^{-/-}$ HSCs because *Nlrp3* deficiency did not affect the bone marrow cellularity, LT-HSC cell number or pyroptosis in *Pnpla2*$^{-/-}$ HSCs (Figures S1F–I). The percentage of cells with ASC specks in *Nlrp3* deficient HSCs was reduced to a level comparable that of wild-type cells (Figure S1J), suggesting that the inflammasome governed *Pnpla2*$^{-/-}$ HSCs were ASC-independent inflammasomes. In all, these results indicate that *Pnpla2* deficiency induces pyroptosis in HSCs.

Pnpla2 knockout triggers HSC exhaustion in a cell-extrinsic manner

In order to find out whether ATGL hindered HSC viability in a cell-intrinsic manner, we firstly examined the self-renewal of *Pnpla2*$^{-/-}$ bone marrow nucleated cells (BMNCs) through a long-term culture initiating cell (LT-CIC) assay. We found that *Pnpla2*$^{-/-}$ BMNCs had a reduced ability of self-renewal (Figure S2A). However, the percentages of cells undergoing pyroptosis between *Pnpla2*$^{+/+}$ and *Pnpla2*$^{-/-}$ BMNC-derived progenitor cells were comparable ((Figures S2B & C). The discrepancy of self-renewals between *Pnpla2*$^{+/+}$ and *Pnpla2*$^{-/-}$ BMNCs might be caused by that there were less HSCs in *Pnpla2*$^{-/-}$ BMNCs than that in *Pnpla2*$^{+/+}$ ones (Figure 1E). We then examined the self-renewal of *Pnpla2*$^{-/-}$ HSCs through the LT-CIC assay. This time, we found that *Pnpla2* knockout did not affect the self-renewal of HSCs (Figure 2A). Moreover, HSC-derived progenitor cells did not undergo pyroptosis (Figures 2B & C). The abilities of colony forming units and the differentiation tendencies were also comparable between *Pnpla2*$^{+/+}$ and *Pnpla2*$^{-/-}$ HSCs (Figures 2D & E). ATGL is responsible for the production of the branched fatty

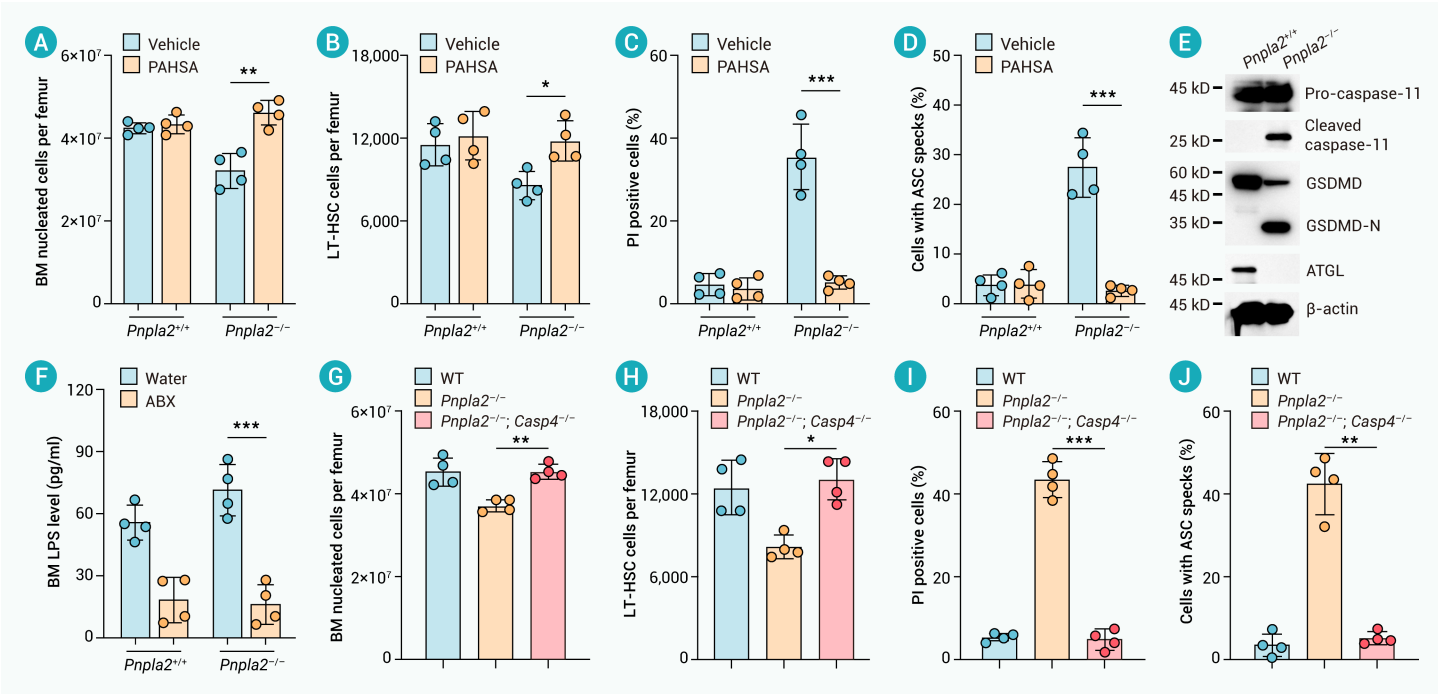

Figure 3. PAHSA suppresses LPS-induced pyroptosis in HSCs (A–D) *Pnpla2*$^{+/+}$ or *Pnpla2*$^{-/-}$ mice were gavaged for 2 weeks with PAHSA at a dose of 30 mg/kg. The cell numbers of BMNCs were calculated using a flow cytometer (A). The cell numbers of LT-HSCs in one femur of the indicated mice were calculated using a flow cytometer (B). LT-HSCs sorted from the indicated mice were stained with PI and the percentages of PI positive cells were calculated (C). LT-HSCs were also stained with antibody against ASC and the percentages of cells with ASC specks were calculated (D). (E) LSK cells sorted from *Pnpla2*$^{+/+}$ or *Pnpla2*$^{-/-}$ mice were subjected to immunoblotting with antibodies against the indicated proteins. (F) *Pnpla2*$^{+/+}$ or *Pnpla2*$^{-/-}$ mice were treated orally with ABX or left untreated for one month. LPS levels in the bone marrow of these mice were examined using an ELISA assay. For ABX treatment, mice were administrated with drinking water containing 1 mg/ml ampicillin, 1 mg/ml gentamicin, 1 mg/ml metronidazole, 1 mg/ml neomycin, 0.5 mg/ml vancomycin, 5 g/L sucrose for one month. (G–J) *Pnpla2*$^{-/-}$ mice were crossed with *Casp11*$^{-/-}$ mice to get the mice deficient for both *Pnpla2* and *Casp11*. The cell numbers of BMNCs in the indicated mice were calculated using a flow cytometer (G). The cell numbers of LT-HSCs in one femur of the indicated mice were calculated using a flow cytometer (H). LT-HSCs sorted from the indicated mice were stained with PI and the percentages of PI positive cells were calculated (I). LT-HSCs were also stained with antibody against ASC and the percentages of cells with ASC specks were calculated (J). Data were shown as means±SD. *, $P < 0.05$; **, $P < 0.01$; ***, $P < 0.001$. Experiments were repeated three times with similar results.

acid PAHSA.[23] We therefore examined the effect of PAHSA to HSC self-renewal. *In vitro* incubation of PAHSA did not affect the self-renewal of HSCs (Figure S2D). PAHSA did not impact on the cell viability of HSCs either (Figures S2E & F). The differentiation tendencies of HSCs were not influenced by the addition of PAHSA (Figure S2G & H).

We then transplanted *Pnpla2*$^{+/+}$ and *Pnpla2*$^{-/-}$ HSCs into WT CD45.1 recipient mice. We found that the reconstitution efficiencies were indistinguishable among *Pnpla2*$^{+/+}$ and *Pnpla2*$^{-/-}$ HSCs (Figures 2F–H). The cell number of *Pnpla2*$^{-/-}$ HSCs was equable to that of *Pnpla2*$^{+/+}$ ones (Figure 2I). *Pnpla2*$^{+/+}$ and *Pnpla2*$^{-/-}$ HSCs had almost the same status of cell viability, in respect of percentages of PI positive cells and cells with ASC specks (Figures 2J & K). We then transplanted WT CD45.1 HSCs to *Pnpla2*$^{+/+}$ and *Pnpla2*$^{-/-}$ mice. We found that donor HSCs had a poor reconstitution ability in *Pnpla2*$^{-/-}$ mice (Figures 2L–N). Moreover, the number of donor-derived HSCs in *Pnpla2*$^{-/-}$ mice was less than that in *Pnpla2*$^{+/+}$ mice (Figure 2O). There were more donor-derived cells undergoing pyroptosis in *Pnpla2*$^{-/-}$ mice than that in *Pnpla2*$^{+/+}$ ones (Figures 2P & Q). These results suggest that *Pnpla2* knockout triggers HSC exhaustion in a cell-extrinsic manner.

PAHSA suppresses HSC pyroptosis and exhaustion *in vivo*

Although PAHSA addition to the HSC culture medium *in vitro* did not affect HSC self-renewal, PAHSA administration to *Pnpla2*$^{-/-}$ mice *in vivo* did restore the bone marrow cellularity to a level comparable to that of wild-type controls (Figure 3A). HSC cell number was also raised in PAHSA-treated *Pnpla2*$^{-/-}$ mice (Figure 3B). Moreover, the percentage of cells undergoing pyroptosis was reduced post PAHSA treatment in *Pnpla2*$^{-/-}$ HSCs (Figures 3C & D). The ASC-independent inflammasome governing HSC viability in *Pnpla2*$^{-/-}$ HSCs (Figure S1J) prompted us to examine the cellular status of the non-canonical inflammasome signaling in *Pnpla2* deficient cells. We found that the non-canonical inflammasome executor caspase-11 was activated in *Pnpla2*$^{-/-}$ LSK cells (Figure 3E). *In vivo* administration of PAHSA blocked the activation of caspase-11 in *Pnpla2*$^{-/-}$ LSK cells (Figure S3A).

LPS from the intestinal bacteria is able to leak into the circulating blood.[32-34] To test the hypothesis that seral LPS induced non-canonical inflammasome activation in HSCs, we firstly examined the LPS levels in the circulating system. We found that LPS did exist in the serum and bone marrow environments (Figures S3B & F). Antibiotics treatment reduced the LPS levels (Figures S3B & F). Antibiotics administration also restored the bone marrow cellularity and HSC cell number of *Pnpla2*$^{-/-}$ mice to levels similar to those of wild-type controls (Figures S3C & D). The percentages of cells undergoing pyroptosis were also diminished in *Pnpla2*$^{-/-}$ mice by antibiotics treatment (Figures S3E & F). Intracellular LPS is recognized by caspase-4/11 and induces non-canonical inflammasome activation.[15,35,36] We generated mice deficient for both *Pnpla2* and *Casp11* (Figure S3G). We found that *Casp11* deficiency restored the cell number of *Pnpla2*$^{-/-}$ bone marrows to a level similar to that of wild-type ones (Figure 3G). LT-HSC cell number of *Pnpla2* and *Casp11* double knockout mice was also elevated to a degree comparable to that of wild-type controls (Figure 3H). What's more, cells undergoing pyroptosis were diminished in these double knockout HSCs when compared with *Pnpla2*$^{-/-}$ cells (Figures 3I & J). In all, these results suggest that PAHSA suppresses HSC pyroptosis and exhaustion *in vivo*.

PAHSA prohibits the binding of HMGB1 to LPS

Given the essential role of caspase-11 in controlling the cell viability of *Pnpla2*$^{-/-}$ HSCs, we examined the intracellular LPS levels in *Pnpla2*$^{+/+}$ or *Pnpla2*$^{-/-}$ HSCs. We found that *in vivo* administration of PAHSA reduced the intracellular LPS levels in *Pnpla2*$^{-/-}$ HSCs (Figure 4A). To find out how PAHSA limited intracellular LPS in HSCs, we firstly examined the association between PAHSA and LPS. We found that 9-PAHSA was able to bind LPS, as well as the lipid A and lipid IVa (Figure 4B), suggesting that the acylated side chains of LPS might be responsible for PAHSA binding. Among the various PAHSA isomers, 9-PAHSA is the most abundant one in mammalian serum.[24,37] 9-PAHSA showed the strongest binding ability to LPS (Figure S4A). Although PAHSA did not bind HMGB1 (Figure S4B), PAHSA prohibited the association

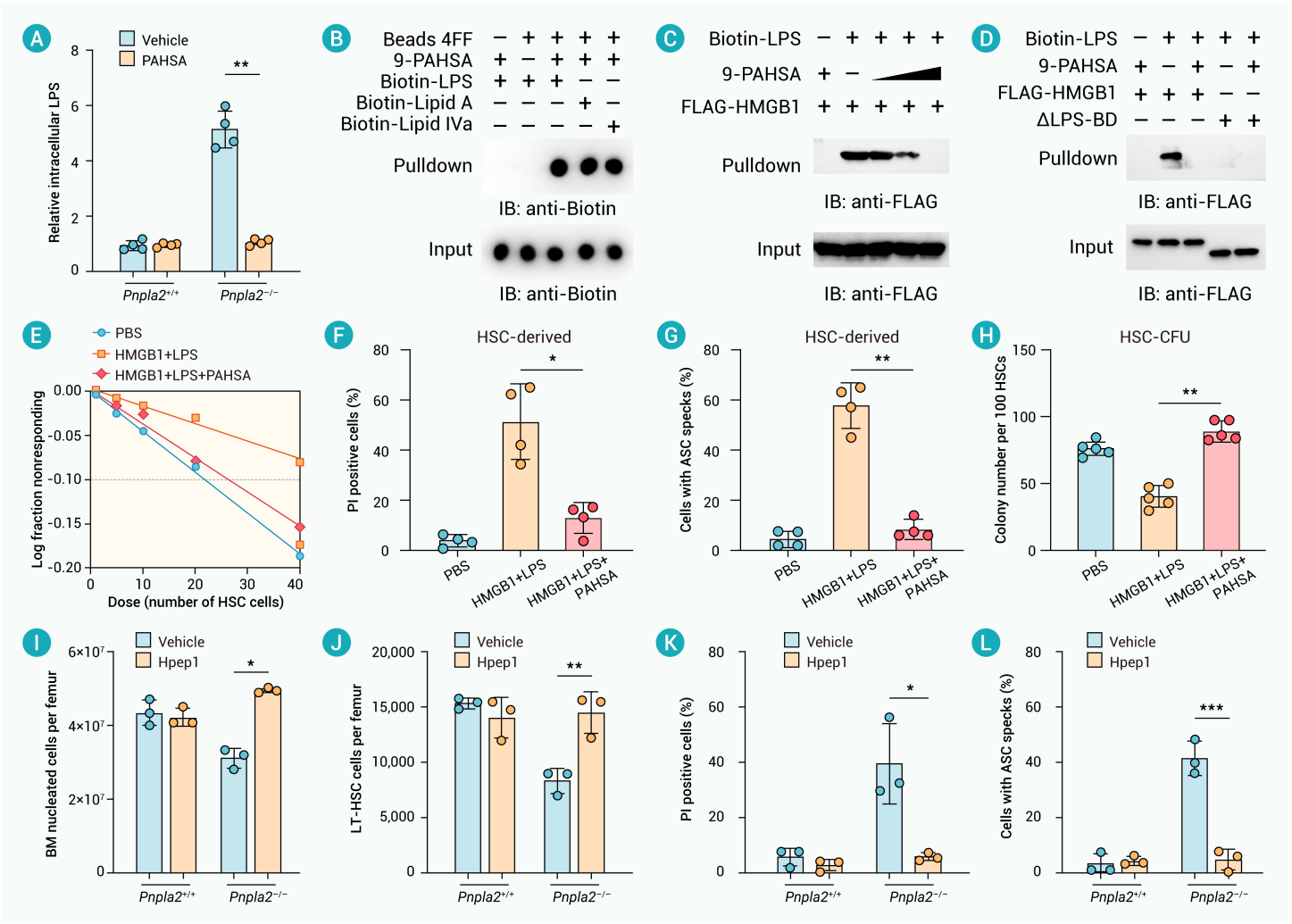

Figure 4. PAHSA hinders the binding of LPS to HMGB1 (A) *Pnpla2*$^{+/+}$ or *Pnpla2*$^{-/-}$ mice were gavaged for 2 weeks with PAHSA at a dose of 30 mg/kg. LPS levels in the LT-HSCs sorted from these mice were examined using an ELISA assay and compared to that of vehicle-treated *Pnpla2*$^{+/+}$ cells. (B) 9-PAHSA immobilized to amino-activated beads 4FF was incubated with biotin-labelled LPS, lipid A or lipid IVa, followed by a pulldown assay. Precipitates were spotted on hydrophobic membranes, followed by blocking with protein-free blocking buffer and immunoblotting with an antibody against biotin. (C) Biotin-LPS was incubated with FLAG-tagged HMGB1 with or without the presence of various concentrations of 9-PAHSA, followed by a pulldown assay. Precipitates and inputs were immunoblotted with an antibody against FLAG. FLAG-tagged HMGB1 was purified from HEK293T cells expressing FLAG-HMGB1. (D) Biotin-LPS was incubated with FLAG-tagged HMGB1 or HMGB1 lacking the LPS-binding domains (DLPS-BD) with or without the presence of 9-PAHSA, followed by a pulldown assay. Precipitates and inputs were immunoblotted with an antibody against FLAG. (E) An LT-CIC assay of WT LT-HSCs treated with or without PAHSA. Sorted HSCs were plated onto irradiated feeder cells with HMGB1, LPS and with or without the presence of PAHSA for 4 weeks, followed by CFU determination. (F, G) WT LT-HSCs were plated onto irradiated feeder cells with HMGB1, LPS and with or without the presence of PAHSA for 4 weeks, followed by digestion into a single cell suspension. Cells with a lymphoid morphology were sorted through a flow cytometric cell sorter. Cells were stained with PI and the percentages of PI positive cells were calculated (F). Cells were also stained with antibody against ASC and the percentages of cells with ASC specks were calculated (G). (H) WT LT-HSCs were cultured with HMGB1, LPS and with or without the presence of PAHSA *in vitro* for CFU determination. CFUs were calculated. (I–L) *Pnpla2*$^{+/+}$ or *Pnpla2*$^{-/-}$ mice were intravenously injected with 100 mg Hpep1 or PBS once every 2 days for 2 weeks. The cell numbers of BMNCs were calculated using a flow cytometer (I). The cell numbers of LT-HSCs in one femur of the indicated mice were calculated using a flow cytometer (J). Sorted LT-HSCs were stained with PI and the percentages of PI positive cells were calculated (K). LT-HSCs were also stained with antibody against ASC and the percentages of cells with ASC specks were calculated (L). Data were shown as means ± SD. *, $P < 0.05$; **, $P < 0.01$; ***, $P < 0.001$. Experiments were repeated three times with similar results.

between HMGB1 and LPS (Figures 4C & S4C). HMGB1 without the LPS-binding domain failed to bind LPS (Figure 4D). HMGB1 binds LPS and enters the cell cytosol with the help of RAGE.[17,38,39] HMGB1 without the RAGE-binding domain bound LPS normally and its binding with LPS was still disturbed by PAHSA (Figure S4D). We then added these HMGB1 variants and LPS to HSCs in the *in vitro* culture system. We found that the intracellular LPS levels were lower in HSCs incubated with these HMGB1 variants than that in cells incubated with WT HMGB1 (Figure S4E), suggesting that HMGB1 was responsible for transporting extracellular LPS into the HSC cytosol.

We then examined the effect of PAHSA *in vitro*. We found that addition of HMGB1 and LPS severely hampered the self-renewal of HSCs in the *in vitro* culturing system, while PAHSA treatment eliminated the effects of HMGB1 and LPS (Figure 4E). PAHSA protected HSCs from pyroptosis caused by HMGB1 and LPS (Figures 4F & G). The colony forming ability was also rescued by PAHSA in HSCs stimulated with HMGB1 and LPS (Figure 4H). However, the differentiation tendencies of HSCs were not influenced by PAHSA (Figure S4F). In mice, the circulating HMGB1 can be suppressed by peptide Hpep1 or glycyrrhizin.[40,41] We found that HMGB1 removal restored bone marrow cellularity in *Pnpla2*$^{-/-}$ mice (Figures 4I & S4G). HSCs were also increased in *Pnpla2* knockout mice post HMGB1 clearance (Figures 4J & S4H). Cells undergoing pyroptosis were diminished in *Pnpla2* knockout HSCs when HMGB1 was removed (Figures 4K, L & S4I, J). Taken together, these results indicate that PAHSA prohibits the binding of HMGB1 to LPS *in vivo*.

PAHSA limits the cytosolic LPS in HSCs

In *Ager* (the gene encoding RAGE) deficient mice (Figure 5A), the intracellular LPS level in HSCs was comparable to that in wild-type mice (Figure 5B). Cell numbers and the pyroptotic status of HSCs were also indistinguishable between *Ager*$^{+/+}$ and *Ager*$^{-/-}$ mice (Figures 5C–E). We then transplanted *Ager*$^{+/+}$ and *Ager*$^{-/-}$ HSCs into *Pnpla2*$^{-/-}$ mice. We found that HSCs deficient for *Ager* had a lower level of intracellular LPS than wild-type cells (Figure 5F). Non-canonical inflammasome activation was also suppressed in *Ager*$^{-/-}$

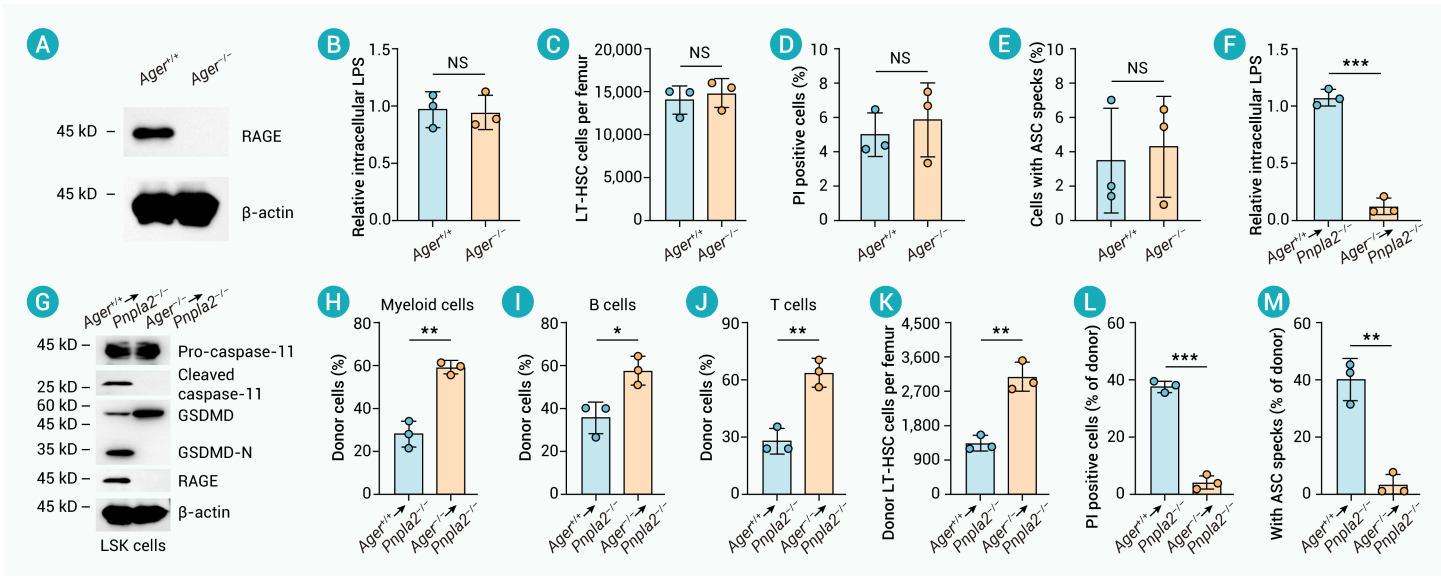

Figure 5. RAGE is required for the entry of LPS into HSCs (A) BMNC cells collected from *Ager*$^{+/+}$ and *Ager*$^{-/-}$ mice were immunoblotted with antibodies against the indicated proteins. (B) LPS levels in the LT-HSCs sorted from *Ager*$^{+/+}$ and *Ager*$^{-/-}$ mice were examined using an ELISA assay and compared to that of *Ager*$^{+/+}$ cells. (C–E) The cell numbers of LT-HSCs in one femur of *Ager*$^{+/+}$ and *Ager*$^{-/-}$ mice were calculated using a flow cytometer (C). LT-HSCs sorted from the indicated mice were stained with PI and the percentages of PI positive cells were calculated (D). LT-HSCs were also stained with antibody against ASC and the percentages of cells with ASC specks were calculated (E). (F, G)100 LT-HSCs sorted from *Ager*$^{+/+}$;tdTomato or *Ager*$^{-/-}$;tdTomato mice were co-transplanted with 3 x 10^5 *Pnpla2*$^{-/-}$ BMNCs into lethally irradiated *Pnpla2*$^{-/-}$ mice for 4 weeks. LPS levels in the donor-derived LT-HSCs sorted from the indicated mice were examined using an ELISA assay and compared to that of *Ager*$^{+/+}$ cells (F). Donor-derived LSK cells were sorted and subjected to immunoblotting with antibodies against the indicated proteins (G). (H–J) 100 LT-HSCs sorted from *Ager*$^{+/+}$;tdTomato or *Ager*$^{-/-}$;tdTomato mice were co-transplanted with 3 x 10^5 *Pnpla2*$^{-/-}$ BMNCs into lethally irradiated *Pnpla2*$^{-/-}$ mice, followed by donor chimerism examination 4 weeks later. (K–M) 100 LT-HSCs sorted from *Ager*$^{+/+}$;tdTomato or *Ager*$^{-/-}$;tdTomato mice were co-transplanted with 3 x 10^5 *Pnpla2*$^{-/-}$ BMNCs into lethally irradiated *Pnpla2*$^{-/-}$ mice for 4 weeks. The cell numbers of donor-derived LT-HSCs in one femur of the indicated mice were calculated using a flow cytometer (K). Donor-derived LT-HSCs were stained with PI and the percentages of PI positive cells were calculated (L). Donor-derived LT-HSCs were also stained with antibody against ASC and the percentages of cells with ASC specks were calculated (M). NS, non-significant. Data were shown as means ± SD. *, $P < 0.05$; **, $P < 0.01$; ***, $P < 0.001$. Experiments were repeated three times with similar results.

LSKs (Figure 5G). *Ager*$^{-/-}$ HSCs had an enhanced reconstitution ability in *Pnpla2*$^{-/-}$ mice than *Ager*$^{+/+}$ cells had (Figures 5H–J). Moreover, the number of *Ager*$^{-/-}$ HSCs in *Pnpla2*$^{-/-}$ mice was more than that of *Ager*$^{+/+}$ cells in *Pnpla2*$^{-/-}$ mice (Figure 5K). There were fewer cells undergoing pyroptosis in *Ager*$^{-/-}$ HSCs than that in *Ager*$^{+/+}$ cells (Figures 5L & M). We then examined the effect of *Ager* deficiency on HMGB1 and LPS stimulation *in vitro*. We found that addition of HMGB1 and LPS severely hampered the self-renewal of *Ager*$^{+/+}$ HSCs but not *Ager*$^{-/-}$ ones (Figure 6A). *Ager* knockout protected HSCs from pyroptosis induced by HMGB1 and LPS (Figures 6B & C). The colony forming ability was also rescued by *Ager* deficiency in HSCs stimulated with HMGB1 and LPS (Figure 6D).

We generated mice deficient for both *Pnpla2* and *Ager* (Figure 6E). We found that *Ager* deficiency restored the cell number of *Pnpla2*$^{-/-}$ bone marrows to a level similar to that of wild-type ones (Figure 6F). The LT-HSC cell number in *Pnpla2* and *Ager* double knockout mice was also elevated to a degree comparable to that of wild-type controls (Figure 6G). What's more, cells undergoing pyroptosis were diminished in these double knockout HSCs when compared with *Pnpla2*$^{-/-}$ cells (Figures 6H & I). In sum, these results suggest that PAHSA limits the cytosolic LPS in HSCs.

PAHSA ameliorates hematopoiesis in obese mice

We observed an enhanced LPS concentration in the serum of obese mice (Figure S5A). Correspondingly, the bone marrow cellularity was decreased in obese mice compared to controls (Figure 7A). Antibiotics treatment restored the seral LPS and the number of bone marrow cells in obese mice to levels similar to those in control mice (Figures S5A & 7A). The HSC cell number was decreased in obese mice and increased post antibiotics treatment (Figure 7B). The number of cells undergoing pyroptosis were increased in obese mice and decreased post antibiotics administration (Figures 7C & D). We then transplanted HSCs from normal or obese mice to WT CD45.1 recipient mice. We found that both of these HSCs showed comparable reconstitution ability (Figures S5B–D). Moreover, the numbers of donor-derived HSCs were nearly equal between these two groups (Figure S5E). There were almost identical percentages of cells undergoing pyroptosis between these two kinds of cells (Figures S5F & G). We then examined the effect of PAHSA administration to the hematopoiesis in obese mice. We found that PAHSA administration to obese mice limited the intracellular LPS concentration in HSCs (Figure S5H). *In vivo* PAHSA-administration restored the bone marrow cellularity of obese mice to a level comparable to that in wild-type controls (Figure 7E). The HSC cell number was also raised in PAHSA-treated obese mice (Figure 7F). Moreover, the percentage of cells undergoing pyroptosis was reduced post PAHSA treatment in HSCs in obese mice (Figure 7G & H).

The addition of HMGB1 and LPS severely hampered the self-renewal of *Casp11*$^{+/+}$ HSCs but not *Casp11*$^{-/-}$ ones (Figure 7I). *Casp11* knockout protected HSCs from pyroptosis induced by HMGB1 and LPS (Figures 7J & K). The colony forming ability was also rescued by *Casp11* deficiency in HSCs stimulated with HMGB1 and LPS (Figure 7L). Moreover, in mice with a *Casp11* deficient background, the bone marrow cellularity was no longer affected by the high-fat diet (Figure S5I). The HSC cell number was not influenced by high-fat diet either (Figure S5J). The percentage of cells undergoing pyroptosis was limited in *Casp11* deficient mice irrespective of the dietary forms (Figure S5K & L). In all, our results indicate that PAHSA ameliorates hematopoiesis in obese mice that rely on the non-canonical inflammasome signaling.

DISCUSSION AND CONCLUSIONS

Here we show that ATGL deficiency leads to HSC pyroptosis and exhaustion. ATGL knockout exerts on HSCs in a cell-extrinsic manner because transplantation of ATGL deficient cells to wild-type mice restores the cell viability of HSCs. Moreover, PAHSA protects HSCs from LPS-induced pyroptosis in in vitro assays. Extracellular LPS binds HMGB1 and enters HSC cytosol, where it activates the caspase-4/11 non-canonical inflammasome. PAHSA binds LPS and hinders the entry of LPS to HSC cytosols through prohibiting the binding of HMGB1 to LPS. Our study uncovers an anti-inflammatory effect of PAHSA in HSCs.

Inflammasomes response to danger signals coming from either inside or outside.[42-44] During infection, HSCs confront danger signals sending from invading pathogens.[45] High levels of endotoxins activate the TLR4 pathway in HSC and lead HSC dysfunction.[9,46,47] Some viral components might also activate inflammasomes in HSCs.[27,48] However, under steady states, the endotoxin from intestinal gram-negative bacteria could also cross the intestinal border and recirculate into the blood.[32,33] How these LPSs were tolerated by

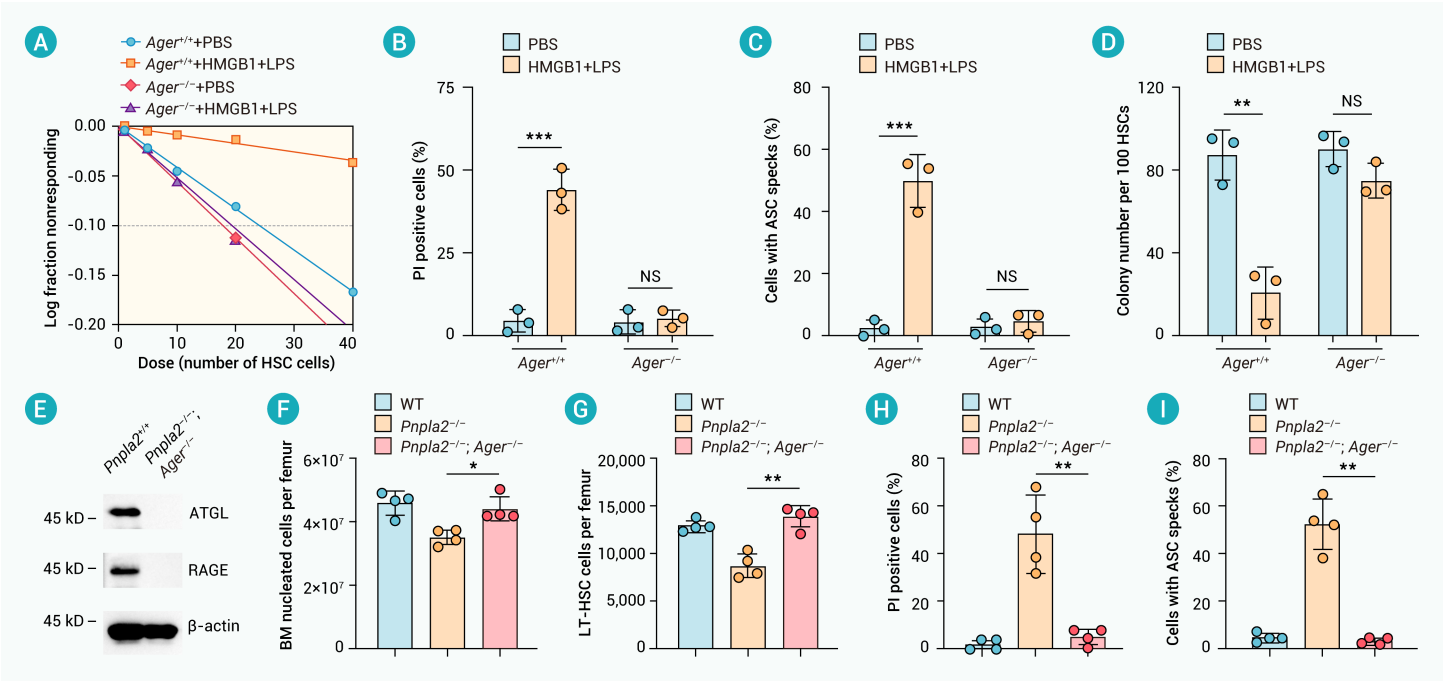

Figure 6. PAHSA limits the intracellular LPS in HSCs (A) An LT-CIC assay of *Ager*$^{+/+}$ and *Ager*$^{-/-}$ LT-HSCs incubated with or without HMGB1 and LPS. Sorted HSCs were plated onto irradiated feeder cells with HMGB1 and LPS for 4 weeks, followed by CFU determination. (B, C) *Ager*$^{+/+}$ and *Ager*$^{-/-}$ LT-HSCs were plated onto irradiated feeder cells with HMGB1 and LPS for 4 weeks, followed by digestion into a single cell suspension. Cells with a lymphoid morphology were sorted through a flow cytometric cell sorter. Cells were stained with PI and the percentages of PI positive cells were calculated (B). Cells were stained with antibody against ASC and the percentages of cells with ASC specks were calculated(C). (D) *Ager*$^{+/+}$ and *Ager*$^{-/-}$ LT-HSCs were cultured with HMGB1 and LPS *in vitro* for CFU determination. The compositions of CFU colonies were examined. (E) BMNC cells collected from *Pnpla2*$^{+/+}$ and *Pnpla2*$^{-/-}$;*Ager*$^{-/-}$ mice were immunoblotted with antibodies against the indicated proteins. (F–I) *Pnpla2*$^{-/-}$ mice were crossed with *Ager*$^{-/-}$ mice to get the mice deficient for both *Pnpla2* and *Ager*. The cell numbers of BMNCs were calculated using a flow cytometer (F). The cell numbers of LT-HSCs in one femur of the indicated mice were calculated using a flow cytometer (G). LT-HSCs sorted from the indicated mice were stained with PI and the percentages of PI positive cells were calculated (H). LT-HSCs were also stained with antibody against ASC and the percentages of cells with ASC specks were calculated (I). NS, non-significant. Data were shown as means ± SD. *, $P < 0.05$; **, $P < 0.01$; ***, $P < 0.001$. Experiments were repeated three times with similar results.

the host to avoid excess immune responses is vital for the host homeostasis. In our study, we find that seral PAHSAs are such a means to constraint the inflammatory effect of the seral LPS. PAHSA binds directly to LPS and hinders the association between HMGB1 and LPS, which is a prerequisite for LPS to enter the cell cytosol. Indeed, seral LPS is such a common contaminant that the host must have adequate ways to eliminate or restrain this hazard. Whether other mechanisms exist to constrain LPS in other non-HSCs are worth further exploration.

Besides the anti-inflammatory effects, PAHSA is long known to have anti-diabetic effects.[24] PAHSA ameliorates the glucose tolerance and stimulates insulin secretion.[25,49] PAHSA also diminishes the inflammation and enhance the glucose uptake in adipose tissues.[23,50] Here, we discover that PAHSA could restore the decreased cell number of HSCs in Pnpla2 deficient mouse. Moreover, PAHSA administration also protects HSCs from pyroptosis in obese mice. The PAHSA levels are diminished in diabetic people,[24,25] suggesting a protective role of this branched fatty acid in regulating glucose metabolism. Whether PAHSA can be used as a drug for the treatment of anti-infection diseases in obese people is a promising research topic in the near future.

In conclusion, the anti-inflammation effect of PAHSA is validated in our study and the LPS-neutralizing ability of PAHSA might be useful for the treatment of sepsis diseases in the clinic in the future.

REFERENCES

1. Laurenti E. and Göttgens B. (2018). From haematopoietic stem cells to complex differentiation landscapes. *Nature* **553**:418–426. DOI:10.1038/nature25022
2. Liggett L. A. and Sankaran V. G. (2020). Unraveling hematopoiesis through the lens of genomics. *Cell* **182**:1384–1400. DOI:10.1016/j.cell.2020.08.030
3. Pinho S. and Frenette P. S. (2019). Haematopoietic stem cell activity and interactions with the niche. *Nat. Rev. Mol. Cell Biol.* **20**:303–320. DOI:10.1038/s41580-019-0103-9
4. Wilkinson A. C., Igarashi K. J. and Nakauchi H. (2020). Haematopoietic stem cell self-renewal in vivo and ex vivo. *Nat. Rev. Genet.* **21**:541–554. DOI:10.1038/s41576-020-0241-0
5. Chavakis T., Mitroulis I. and Hajishengallis G. (2019). Hematopoietic progenitor cells as integrative hubs for adaptation to and fine-tuning of inflammation. *Nat. Immunol.* **20**:802–811. DOI:10.1038/s41590-019-0402-5
6. Schultze J. L., Mass E. and Schlitzer A. (2019). Emerging principles in myelopoiesis at homeostasis and during infection and inflammation. *Immunity* **50**:288–301. DOI:10.1016/j.immuni.2019.01.019
7. Wei Q. and Frenette P. S. (2018). Niches for hematopoietic stem cells and their progeny. *Immunity* **48**:632–648. DOI:10.1016/j.immuni.2018.03.024
8. Pietras E. M., Mirantes-Barbeito C., Fong S., et al. (2016). Chronic interleukin-1 exposure drives haematopoietic stem cells towards precocious myeloid differentiation at the expense of self-renewal. *Nat. Cell. Biol.* **18**:607–618. DOI:10.1038/ncb3346
9. Takizawa H., Fritsch K., Kovtonyuk L. V., et al. (2017). Pathogen-induced TLR4-TRIF innate immune signaling in hematopoietic stem cells promotes proliferation but reduces competitive fitness. *Cell Stem Cell* **21**:225–240.e225. DOI:10.1016/j.stem.2017.06.013
10. Mistry J. J., Hellmich C., Moore J. A., et al. (2021). Free fatty-acid transport via CD36 drives β-oxidation-mediated hematopoietic stem cell response to infection. *Nat. Commun.* **12**:7130. DOI:10.1038/s41467-021-27460-9
11. Ratajczak M. Z. and Kucia M. (2022). Hematopoiesis and innate immunity: An inseparable couple for good and bad times, bound together by an hormetic relationship. *Leukemia* **36**:23–32. DOI:10.1038/s41375-021-01482-0
12. Xia J., Shen L., Liu Y., et al. (2025). Ace2 safeguards embryonic hematopoietic stem and progenitor cell production by restraining Nlrp3-mediated pyroptosis. *Proc. Natl. Acad. Sci. USA* **122**:e2515641122. DOI:10.1073/pnas.2515641122
13. Newton K., Dixit V. M. and Kayagaki N. (2021). Dying cells fan the flames of inflammation. *Science* **374**:1076–1080. DOI:10.1126/science.abi5934
14. Zhu F., Ma J., Li W., et al. (2023). The orphan receptor Nur77 binds cytoplasmic LPS to activate the non-canonical NLRP3 inflammasome. *Immunity* **56**:753–767.e758. DOI:10.1016/j.immuni.2023.03.003
15. Vanaja S. K., Russo A. J., Behl B., et al. (2016). Bacterial outer membrane vesicles mediate cytosolic localization of LPS and caspase-11 activation. *Cell* **165**:1106–1119. DOI:10.1016/j.cell.2016.04.015
16. Qian Y., Liu Q., Cheng X., et al. (2025). A VgrG2b fragment cleaved by caspase-11/4 promotes Pseudomonas aeruginosa infection through suppressing the NLRP3 inflammasome. *elife* **13**:RP99939. DOI:10.7554/eLife.99939
17. Deng M., Tang Y., Li W., et al. (2018). The endotoxin delivery protein HMGB1 mediates caspase-11-dependent lethality in sepsis. *Immunity* **49**:740–753.e7. DOI:10.1016/j.immuni.2018.08.016
18. Tang Y., Wang X., Li Z., et al. (2021). Heparin prevents caspase-11-dependent septic lethality independent of anticoagulant properties. *Immunity* **54**:454–467.e456. DOI:10.

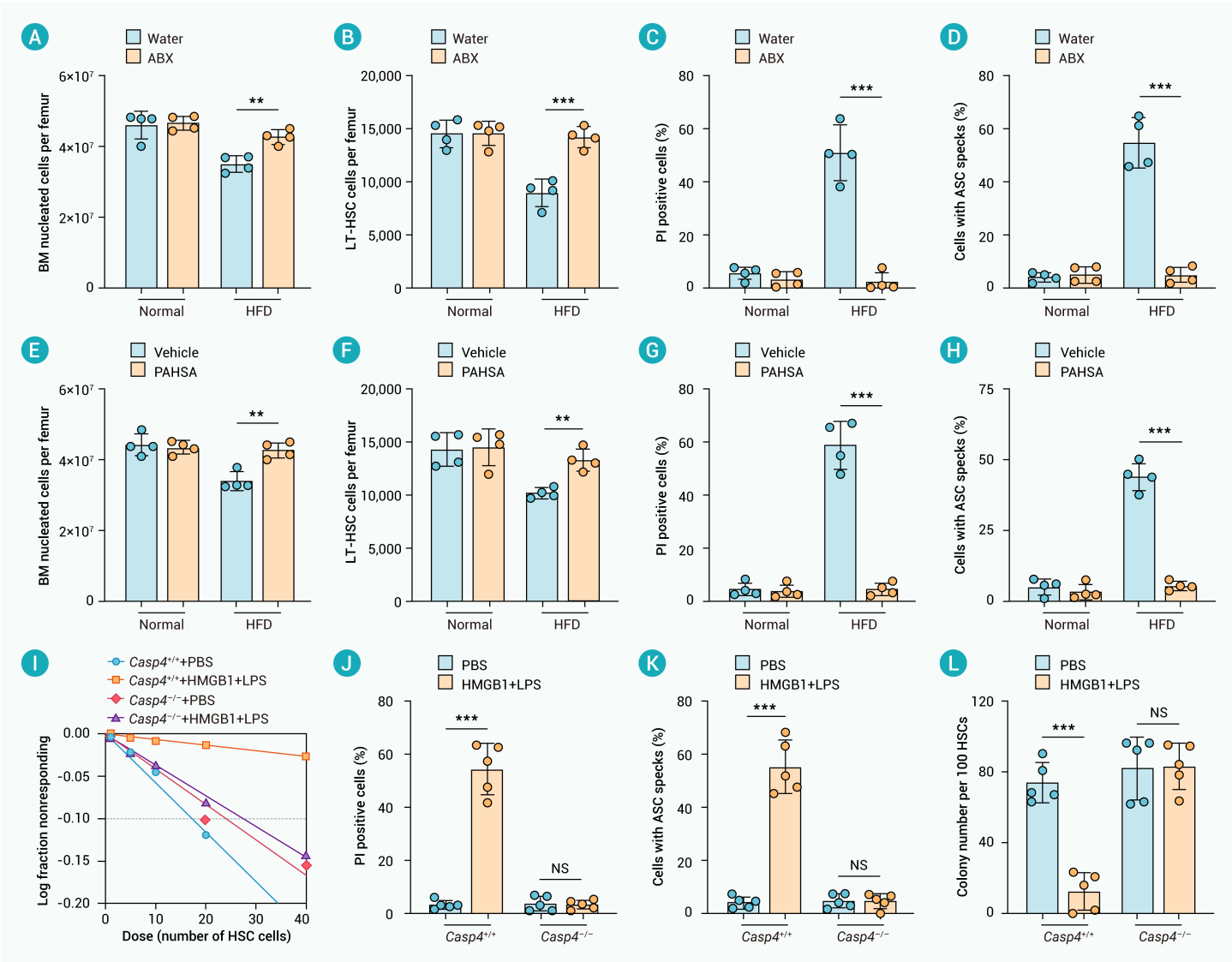

Figure 7. PAHSA protects HSCs from pyroptosis in obese mice (A–D) WT mice were fed with a standard diet or high-fat diet (HFD) for 10 weeks. One month before the mice were sacrificed, mice were treated orally with ABX or left untreated. The cell numbers of BMNCs were calculated using a flow cytometer (A). The cell numbers of LT-HSCs in one femur of the indicated mice were calculated using a flow cytometer (B). LT-HSCs sorted from the indicated mice were stained with PI and the percentages of PI positive cells were calculated (C). LT-HSCs were also stained with antibody against ASC and the percentages of cells with ASC specks were calculated (D). (E–H) WT mice were fed with a standard diet or high-fat diet (HFD) for 10 weeks. Mice were gavaged for 2 weeks with PAHSA at a dose of 30 mg/kg before the mice were sacrificed. The cell numbers of BMNCs were calculated using a flow cytometer (E). The cell numbers of LT-HSCs in one femur of the indicated mice were calculated using a flow cytometer (F). LT-HSCs sorted from the indicated mice were stained with PI and the percentages of PI positive cells were calculated (G). LT-HSCs were also stained with antibody against ASC and the percentages of cells with ASC specks were calculated (H). (I) An LT-CIC assay of *Casp11*$^{+/+}$ and *Casp11*$^{-/-}$ LT-HSCs incubated with or without HMGB1 and LPS. HSCs sorted from the indicated mice were plated onto irradiated feeder cells with HMGB1 and LPS for 4 weeks, followed by CFU determination. (J, K) *Casp11*$^{+/+}$ and *Casp11*$^{-/-}$ LT-HSCs were plated onto irradiated feeder cells with HMGB1 and LPS for 4 weeks, followed by digestion into a single cell suspension. Cells with a lymphoid morphology were sorted through a flow cytometric cell sorter. Cells were stained with PI and the percentages of PI positive cells were calculated (J). Cells were also stained with antibody against ASC and the percentages of cells with ASC specks were calculated (K). (L) *Casp11*$^{+/+}$ and *Casp11*$^{-/-}$ LT-HSCs were cultured with HMGB1 and LPS *in vitro* for CFU determination. The compositions of CFU colonies were examined. NS, non-significant. Data were shown as means ± SD. **, $P < 0.01$; ***, $P < 0.001$. Experiments were repeated three times with similar results.

1016/j.immuni.2021.01.007

19. Shi J., Zhao Y., Wang Y., et al. (2014). Inflammatory caspases are innate immune receptors for intracellular LPS. *Nature* **514**:187–192. DOI:10.1038/nature13683
20. Chen Y., Qin X., An Q., et al. (2018). Mesenchymal stromal cells directly promote inflammation by canonical NLRP3 and non-canonical caspase-11 inflammasomes. *EBioMedicine* **32**:31–42. DOI:10.1016/j.ebiom.2018.05.023
21. Brejchova K., Radner F. P. W., Balas L., et al. (2021). Distinct roles of adipose triglyceride lipase and hormone-sensitive lipase in the catabolism of triacylglycerol estolides. *Proc. Natl. Acad. Sci. USA* **118**. DOI:10.1073/pnas.2020999118
22. Li W., Liu Q., Qian Y., et al. (2024). Adipose triglyceride lipase suppresses noncanonical inflammasome by hydrolyzing LPS. *Nat. Chem. Biol.* **20**:1434–1442. DOI:10.1038/s41589-024-01569-6
23. Patel R., Santoro A., Hofer P., et al. (2022). ATGL is a biosynthetic enzyme for fatty acid esters of hydroxy fatty acids. *Nature* **606**:968–975. DOI:10.1038/s41586-022-04787-x
24. Yore M. M., Syed I., Moraes-Vieira P. M., et al. (2014). Discovery of a class of endogenous mammalian lipids with anti-diabetic and anti-inflammatory effects. *Cell* **159**:318–332. DOI:10.1016/j.cell.2014.09.035
25. Syed I., Lee J., Moraes-Vieira P. M., et al. (2018). Palmitic acid hydroxystearic acids activate GPR40, which is involved in their beneficial effects on glucose homeostasis. *Cell Metab.* **27**:419–427.e414. DOI:10.1016/j.cmet.2018.01.001
26. Yang Q., Vijayakumar A. and Kahn B. B. (2018). Metabolites as regulators of insulin sensitivity and metabolism. *Nat. Rev. Mol. Cell Biol.* **19**:654–672. DOI:10.1038/s41580-018-0044-8
27. Masters S. L., Gerlic M., Metcalf D., et al. (2012). NLRP1 inflammasome activation induces pyroptosis of hematopoietic progenitor cells. *Immunity* **37**:1009–1023. DOI:10.1016/j.immuni.2012.08.027
28. Shi J., Zhao Y., Wang K., et al. (2015). Cleavage of GSDMD by inflammatory caspases determines pyroptotic cell death. *Nature* **526**:660–665. DOI:10.1038/nature15514
29. Miao R., Jiang C., Chang W. Y., et al. (2023). Gasdermin D permeabilization of mitochondrial inner and outer membranes accelerates and enhances pyroptosis. *Immunity* **56**:2523–2541.e2528. DOI:10.1016/j.immuni.2023.10.004
30. Hu J. J., Liu X., Xia S., et al. (2020). FDA-approved disulfiram inhibits pyroptosis by blocking gasdermin D pore formation. *Nat. Immunol.* **21**:736–745. DOI:10.1038/s41590-020-0669-6
31. Wang C., Yang T., Xiao J., et al. (2021). NLRP3 inflammasome activation triggers

gasdermin D-independent inflammation. *Sci. Immunol.* **6**:eabj3859. DOI:10.1126/sciimmunol.abj3859
32. Mandal P., Feng Y., Lyons J. D., et al. (2018). Caspase-8 collaborates with caspase-11 to drive tissue damage and execution of endotoxic shock. *Immunity* **49**:42–55.e46. DOI:10.1016/j.immuni.2018.06.011
33. Yang X., Cheng X., Tang Y., et al. (2019). Bacterial endotoxin activates the coagulation cascade through gasdermin D-dependent phosphatidylserine exposure. *Immunity* **51**:983–996.e986. DOI:10.1016/j.immuni.2019.11.005
34. Wei C., Jiang W., Wang R., et al. (2024). Brain endothelial GSDMD activation mediates inflammatory BBB breakdown. *Nature* **629**:893–900. DOI:10.1038/s41586-024-07314-2
35. Rathinam V. A. K., Zhao Y. and Shao F. (2019). Innate immunity to intracellular LPS. *Nat. Immunol.* **20**:527–533. DOI:10.1038/s41590-019-0368-3
36. Wang K., Sun Q., Zhong X., et al. (2020). Structural mechanism for GSDMD targeting by autoprocessed caspases in pyroptosis. *Cell* **180**:941–955.e920. DOI:10.1016/j.cell.2020.02.002
37. Kuda O., Brezinova M., Silhavy J., et al. (2018). Nrf2-mediated antioxidant defense and peroxiredoxin 6 are linked to biosynthesis of palmitic acid ester of 9-hydroxystearic acid. *Diabetes* **67**:1190–1199. DOI:10.2337/db17-1087
38. Gong T., Liu L., Jiang W., et al. (2020). DAMP-sensing receptors in sterile inflammation and inflammatory diseases. *Nat. Rev. Immunol.* **20**:95–112. DOI:10.1038/s41577-019-0215-7
39. Wang Y., Luo W., Han J., et al. (2020). MD2 activation by direct AGE interaction drives inflammatory diabetic cardiomyopathy. *Nat. Commun.* **11**:2148. DOI:10.1038/s41467-020-15978-3
40. Ren Y., Cao L., Wang L., et al. (2021). Autophagic secretion of HMGB1 from cancer-associated fibroblasts promotes metastatic potential of non-small cell lung cancer cells via NFκB signaling. *Cell Death Dis.* **12**:858. DOI:10.1038/s41419-021-04150-4
41. Fu Y., Xiang Y., Wang Y., et al. (2023). The STAT1/HMGB1/NF-κB pathway in chronic inflammation and kidney injury after cisplatin exposure. *Theranostics* **13**:2757–2773. DOI:10.7150/thno.81406
42. Barnett K. C., Li S., Liang K., et al. (2023). A 360° view of the inflammasome: Mechanisms of activation, cell death, and diseases. *Cell* **186**:2288–2312. DOI:10.1016/j.cell.2023.04.025
43. Sundaram B., Tweedell R. E., Prasanth Kumar S., et al. (2024). The NLR family of innate immune and cell death sensors. *Immunity* **57**:674–699. DOI:10.1016/j.immuni.2024.03.012
44. Liu Q., Tang Z., Qian Y., et al. (2025). Eukaryotic ADCY7 catalyzes the production of c-di-AMP to activate the NLRP3 inflammasome. *Nat. Chem. Biol.* **21**:1283–1291. DOI:10.1038/s41589-025-01919-y
45. Khan N., Downey J., Sanz J., et al. (2020). M.tuberculosis reprograms hematopoietic stem cells to limit myelopoiesis and impair trained immunity. *Cell* **183**:752–770.e722. DOI:10.1016/j.cell.2020.09.062
46. Carnevalli L. S., Scognamiglio R., Cabezas-Wallscheid N., et al. (2014). Improved HSC reconstitution and protection from inflammatory stress and chemotherapy in mice lacking granzyme B. *J. Exp. Med.* **211**:769–779. DOI:10.1084/jem.20131072
47. Vanickova K., Milosevic M., Ribeiro Bas I., et al. (2023). Hematopoietic stem cells undergo a lymphoid to myeloid switch in early stages of emergency granulopoiesis. *Embo j* **42**:e113527. DOI:10.15252/embj.2023113527
48. Ratajczak M. Z., Bujko K., Ciechanowicz A., et al. (2021). SARS-CoV-2 entry receptor ACE2 is expressed on very small CD45(-) precursors of hematopoietic and endothelial cells and in response to virus spike protein activates the Nlrp3 inflammasome. *Stem Cell Rev. Rep.* **17**:266–277. DOI:10.1007/s12015-020-10010-z
49. Choi B. S., Daniel N., Houde V. P., et al. (2021). Feeding diversified protein sources exacerbates hepatic insulin resistance via increased gut microbial branched-chain fatty acids and mTORC1 signaling in obese mice. *Nat. Commun.* **12**:3377. DOI:10.1038/s41467-021-23782-w
50. Paluchova V., Oseeva M., Brezinova M., et al. (2020). Lipokine 5-PAHSA is regulated by adipose triglyceride lipase and primes adipocytes for De Novo lipogenesis in mice. *Diabetes* **69**:300–312. DOI:10.2337/db19-0494

FUNDING AND ACKNOWLEDGMENTS

We thank Ting Li (Peking University) for technical help. This work was supported by the National Natural Science Foundation of China (92369104, 82271790, 92169113, 22174003, 92569301, 82595923 and U25A20654), Beijing Natural Science Foundation (JG23028), the National Key R&D Program of China (2022YFC2302900), Strategic Priority Research Programs of the Chinese Academy of Sciences (XDB29020000), Key Research Program of Frontier Sciences of Chinese Academy of Sciences (ZDBS-LY-SM025), CAS Project for Young Scientists in Basic Research (YSBR-010), the Science and Technology Project of Beijing Life Science Academy (2025500CC0180). Fok Ying Tung Education Foundation to P.X., Youth Innovation Promotion Association of CAS to S.W..The funders had no role in study design, data collection and analysis, decision to publish, or preparation of the manuscript.

AUTHOR CONTRIBUTIONS

Y.Q. and Q.L. designed and performed experiments and analyzed data; Y.Z. and S.W. performed experiments and analyzed data; S.W. and P.X. initiated the study, designed and performed experiments, analyzed data, and wrote the paper. All authors contributed to the manuscript and approved the final version.

DECLARATION OF INTERESTS

The authors declare no competing interests.

ETHICAL STATEMENT AND PATIENT CONSENT

This study was licensed by the Biomedical Ethics Committee of Peking University (LA2022080), Institutional Animal Care and Use Committee of Peking University Health Science Center (BCJE0167) and Ethics Committee of the Institute of Microbiology, Chinese Academy of Sciences (CAS). Our research complies with all relevant ethical regulations.

DATA AND CODE AVAILABILITY

Data are available from the corresponding author upon reasonable request.

SUPPLEMENTAL INFORMATION

It can be found online at https://doi.org/10.59717/j.xinn-life.2026.100178